Development of a headlight glare simulator for a driving simulator

Alex D. Hwang *, Eli Peli

Schepens Eye Research Institute, Massachusetts Eye and Ear, Department of Ophthalmology, Harvard Medical School, Boston, MA, USA

ARTICLE INFO

ABSTRACT

We describe the design and construction of a headlight glare simulator to be used with a driving simulator. The system combines a modified programmable off-the-shelf LED display board and a beamsplitter so that the LED lights, representing the headlights of oncoming cars, are superimposed over the driving simulator headlight images. Ideal spatial arrangement of optical components to avoid misalignments of the superimposed images is hard to achieve in practice, and variations inevitably introduce some parallax. Furthermore, driver's viewing position varies with driver height and seating position preferences, exacerbating misalignment. We reduce the parallax errors using an intuitive calibration procedure (a simple drag-and-drop alignment of nine LED positions with calibration dots on the screen). To simulate the dynamics of headlight brightness changes when two vehicles are approaching, LED intensity control algorithms based on both headlight and LED beam shapes were developed. The simulation errors were estimated and compared favorably with real-world headlight brightness variability.

© 2012 Elsevier Ltd. All rights reserved.

1. Introduction

Glare is the visual effect of scattering light within (or in front of) the eye caused by a relatively bright light source in the field of view (Miller and Benedek, 1973; Van den Berg et al., 2009). The scattered light (veiling) reduces retinal contrast across the visual field and thus reduces overall visibility (disability glare), in addition to causing distraction and annoyance (discomfort glare). If the glare is strong, it may cause total wash-out of the scene. The contrast reduction makes it difficult to perform various visual tasks related to driving, such as detecting pedestrians (Wood et al., 2012), detecting other on-road objects, and following the lane. Disability glare as well as discomfort glare caused by oncoming headlights has been associated with nighttime traffic accidents (Bullough et al., 2008; Plainis et al., 2005). Although headlight glare cannot be considered as a sole factor of all nighttime driving accidents, it is known that pedestrians are much more at risk of fatal collisions in the dark (Sullivan and Flannagan, 2002), and the proportion of drivers involved in such collisions increases with age of the driver (Owens and Brooks, 1995). Even though there are many other effects of aging such as slower reaction time and cognitive decline that may affect the driving performance of older drivers, they are more susceptible to glare due to changes in their eye's media, especially the crystalline lens (Owsley et al., 2012). Therefore, oncoming headlight glare could be a significant risk factor.

As the population ages, oncoming headlight glare will likely become more of a problem, yet little is currently known about the functional impact or behavioral response to oncoming headlight glare. As the eye's crystalline lens develops age-related opacities (cataract), light scattering increases with consequential glare/veiling effects (De Waard et al., 1992;

* Corresponding author. Present address: Schepens Eye Research Institute, 20 Staniford Street, Boston, MA 02114, USA. Tel.: +1 919 617 1004; fax: +1 617 912 0112.
E-mail addresses: alex.hwang@schepens.harvard.edu (A.D. Hwang), eli.peli@schepens.harvard.edu (E. Peli).

Sjostrand et al., 1987). Furthermore, people with age-related macular degeneration (AMD) have impaired dark adaptation (Sandberg and Gaudio, 1995), thus they may experience the glare/veiling effect for longer than the actual glare exposure duration, and are likely to be more adversely affected by headlight glare (Collins, 1989). With the increase of both life expectancy and mobility in older age groups, the number of people with cataract and/or early AMD symptoms who are driving is expected to increase rapidly.

Ophthalmic devices such as implanted multifocal intra ocular lenses and multifocal contact lenses cause light scatter seen as halos. Clinical studies show that the patients with such devices exhibit greater glare effect (Akutsu et al., 1993; Winther-Nielson et al., 1993). However, it is not clear how this increased glare affects real-life tasks like nighttime driving. Therefore, a greater understanding of the impact of headlight glare under such conditions could improve road safety for road users of all ages and help to improve designs of these devices to reduce the impact of the glare effects.

The need to understand the functional impact of the headlight glare has led to numerous studies. Flannagan (1999) measured the subjective glare response (glare rating) and luminance threshold for detecting a target (pedestrian silhouette) that appeared in front of the subject while glare sources are fixed to the left and right of the target. He found that the size and color of the headlight affected subjective level of discomfort glare, but not the functional disability glare performance. Akashi and Rea (2001) used a parked car to provide oncoming headlight glare while the subject's car was parked across. Subjects were asked to detect an illuminating target appearing at certain distances and angles. Surprisingly, they found that the presence of the oncoming headlight delayed the target detection for the large eccentricity target but not for the small eccentricity target. Bullough et al. (2002) conducted a set of indoor experiments in which three types of real headlamp were placed at two different off-axis angles and three light levels and measured the visibility (contrast threshold) of targets. They found that both light level and viewing angle for the glare source were significant factors for the target visibility, while the type of the headlamp which varied in spectral contents did not affect the target visibility significantly. Shi et al. (2008) employed a similar experimental setting and found no benefit of a tinted windshield for the subject's glare performance.

Although the experimental designs were appropriate for measuring the impact of the glare itself, since most studies have relied on static glare sources and stationary driver's car, the results cannot easily be translated to real-world impact on driving condition, where the oncoming headlight continuously changes its brightness and position relative to the driver. Also, the target (pedestrian) was often fixed, and the tasks were not accompanied by common cognitive loads and attention strategy related to driving. We argue that it is preferable that headlight glare response be measured within a realistic driving environment like a driving simulator, along with proper simulation of oncoming headlight glare to increase the applicability of the results.

To design a headlight glare simulator that works with a driving simulator, the system needs to be compact, and the position and brightness of the light source need to be controlled quickly and accurately. Conventional headlight sources (e.g., halogen lamps) are big and heavy, making it difficult to control their position and brightness. Furthermore, the beam shape of a chosen headlight source (lamp/reflector) only represents a particular model, and may limit the measured effect to the particular headlight type used.

The dynamic nature of an oncoming car's headlight glare has not been studied much because of the difficulties of realistic glare simulation. A prototype headlight glare simulator to be used with a driving simulator was developed in our lab (Fullerton and Peli, 2009). The system combined an off-the-shelf programmable LED display board and a beamsplitter so that the LED lights are superimposed over the driving simulator's screen. The positions of illuminated LEDs are spatially synchronized with the on-screen positions of simulated oncoming traffic's movements, and the light intensities of LEDs are also matched to real world headlight intensities as visible to a driver. Although the early prototype headlight glare simulator proved the feasibility of the concept, and simulated the light levels and the dynamics of the headlight movements to some degree, the system had various limitations we addressed here.

The earlier prototype design required precise alignments of its components. The LCD screen of the driving simulator and the LED display board of the glare simulator had to be installed perpendicular to each other, and the beamsplitter had to be positioned at exactly 45° between them. Due to the tight space between LCD screen and driver, this ideal set-up was hard to achieve and maintain in practice. If the ideal positioning of the LCD screen, LED board, and beamsplitter is not maintained, the misalignment introduces parallax. Due to the relatively short distance between the image-merging surface (beamsplitter) and the driver's viewing position, even a small amount of misalignment of the parts becomes noticeable at off-center screen locations. Since viewing position varies between drivers, due to each driver's height and seating position preferences, the magnitude and the direction of misalignments also vary individually, and prevent the use of static, system-wide, mapping corrections. To minimize the misalignments caused by parallax, we have implemented an intuitive individual calibration procedure (a simple drag-and-drop of on-screen calibration dots) which defines a set of spatial mapping coefficients for each driver. In addition to the improvements in spatial synchronization, in order to simulate the dynamics of headlight brightness changes during nighttime driving, new LED intensity control algorithms based on real-world headlights and LED beam shapes were developed and validated.

The improved headlight glare simulator is a valuable tool for testing the impact of headlight glare for drivers of different ages and vision conditions, as well as for evaluating the possible glare effects of variety of vision aids, such as multifocal contact lenses and intraocular lens implants, surgical procedures such as LASIK, and mitigation devices or treatment of increasing macular pigment which can decrease glare effects (Stringham and Hammond, 2008) during nighttime driving.
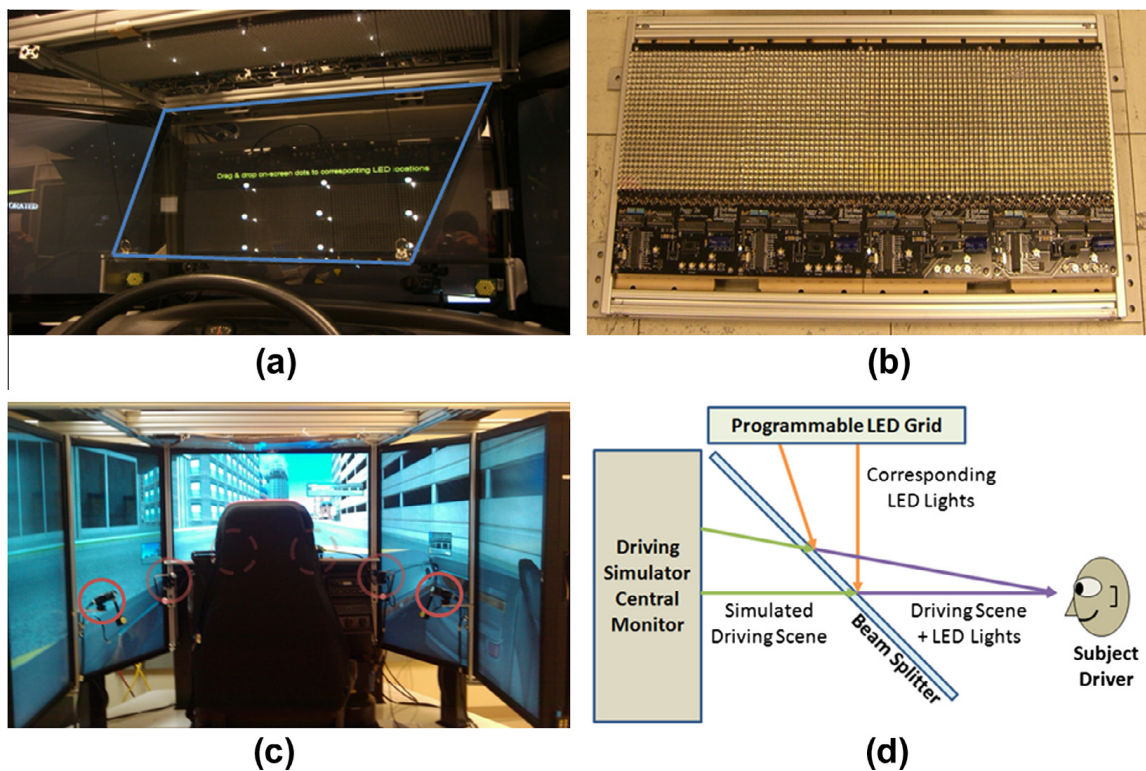
2. Configuration of the headlight glare simulator

The headlight glare simulator system integrates a driving simulator (LE-1500 from FAAC, Inc., Ann Arbor, MI, Fig. 1a), a custom-modified programmable LED display board module (Peggy 2LE programmable LED boards from Evil Mad Science Laboratory, evilmadscience.com, Fig. 1b), and a beamsplitter plate (Acrylic see-through mirror from Reflection Products, Inc., Roswell, GA, Fig. 1c), optically aligned as shown in Fig. 1d with our custom-designed software.

The driving simulator has five 42″ LCD monitors, and they are spatially arranged to span 225° of the driver's field of view (horizontally). The central monitor provides a 68.2° (horizontal) × 43.5° (vertical) view of the scene in front of the vehicle. The driving simulator has a force feedback steering wheel, and a motion seat with three degrees of freedom to provide a more realistic driving experience. It comes with a 1600 m × 800 m virtual world containing urban and rural areas. A scenario development tool box allows us to design test drive scenarios and create precise task-related events for various experimental conditions, including pedestrian movements, autonomous vehicle (traffic) driving paths, and location/timing-based event triggering. During experiments, the driving simulator produces a 30 Hz real-time data stream which contains locations and orientations of all scripted objects and the driver's car in the virtual world. We use the data stream to link our headlight glare simulation in real time to the scene. A 6-camera remote eye and head tracking system from SmartEye AB (Goteborg, Sweden) was installed in the driving simulator. The Smart Eye system allows us to track both head and eye movements across the total field of view (225°) encompassed by the simulator monitors, with an accuracy of 1°. The eye tracking signal is synchronized to the simulator scenario data recorded.

The LED display module is composed of four programmable LED custom display boards. Each board has a 25 × 25 array of high intensity LEDs (5 mm diameter) installed on a tight grid covering 0.15 m × 0.15 m. The locations and brightness levels of the LEDs to be lit are controlled through a USB connection. The side wall of each LED was individually shielded to prevent lateral light leakages between the LEDs. The use of an external glare source (LEDs) is required because conventional LCD screens used in the driving simulator produce less than 200 candelas per square meter (cd/m^2), which is not bright enough to simulate the brightness of real-world headlights. Although an LCD screen can be used to draw the shape of a simulated glare source with white pixels, they do not induce the actual glare effect in the driver's eyes.

A beamsplitter, also commonly known as a "half-silvered mirror" or "teleprompter mirror", has optical characteristics of both transparency and reflectance. The T/R ratio describes how much light incident to the beamsplitter will be reflected, and how much light will pass through it. For example, a $40T/60R$ beamsplitter reflects 60% of the incident-light and allows 40% of the incident-light to pass through it. In particular, if a beamsplitter is aligned in 45° between two light sources (LCD screen

Fig. 1. Components of the headlight glare simulator. (a) The 5-LCD screen driver training simulator. The locations of eye tracker cameras are circled. (b) Custom programmable LED boards (note that 4 LED boards were combined to form a 25 × 100 maximally packed LED grid). (c) 42T/58R acrylic beamsplitter plate hanging from the ceiling compartment. A blue outline is added for visibility. (d) Schematic of the headlight glare simulator. Lights from the two sources are combined by the beamsplitter and presented to the driver. (For interpretation of the references to color in this figure legend, the reader is referred to the web version of this article.)

and LED display), as shown in Fig. 1d, simulated driving scenes displayed on the driving simulator screen are visible through the beamsplitter. The LED lights installed on the upper (i.e., "ceiling") surface of the driving simulator produce bright light directed downward. These lights are reflected on the beamsplitter surface. Therefore, a viewer (driver) sees a superimposed image of the LED lights over the simulated scene. This simple optical configuration allows the placement of a bright light source that does not obstruct the driving simulator display. For the headlight glare simulator described in this paper, a $42T/58R$ acrylic beamsplitter was used.

3. Spatial alignments of two light sources

As briefly mentioned in the previous section, the headlight glare simulator combines lights from two sources, an LCD screen and an LED grid, aligned approximately perpendicularly to each other, using a beamsplitter. A precise alignment of onscreen headlights and the corresponding LEDs to be lit is crucial for the successful headlight glare simulation. Under ideal conditions, where the beamsplitter is aligned at exactly 45° between two exactly perpendicular light sources, and the two light sources are placed at an equal distance from the beamsplitter, perfect alignments will be accomplished. However, due to physical space limitation of the driving simulator, this ideal setting is hard to achieve. For example, the lower edge of a 45° slanted beam splitter may be too close to the steering wheel and limit the driver's steering movements. Therefore, the beamsplitter position needs to be adjusted for each driver's seating preference, and the misalignments caused by this adjustment introduce parallax. To reduce this problem, we have developed a simple calibration process that generates a spatial mapping function between two light source planes for each driver. Below we discuss our general assumptions about the driving simulator's coordinate system and how our calibration/mapping procedure helps convert the oncoming car's headlight positions in the virtual world to the best matching LED grid coordinates.

3.1. Computing onscreen headlight locations in pixels

The driving simulator renders a view of the virtual world onto each corresponding screen based on an assumption that a driver's view point is located at a specific location in the physical world (0.735 m away from the center of the central screen). This fixed driver's view point makes rendering and designing of the driving simulator system much simpler because it means that the only dynamic factors that affect onscreen views of the driving scene are limited to the orientation and location of the driver's car and other objects in the virtual world. This, however, can be considered as a limitation of the simulation because the views drawn on the LCD screens are not adjusted in response to changes in driver's head position. While this results in imperfect simulation, it is usually not a problem because the driver's lateral head movements during the driving are generally small. It has been shown that drivers make lateral head movements of 2 in. on average when looking at the side mirrors, and make a median 1.5 in. movement while making turns (Bhise et al., 1981). Since objects displayed on the screens are positioned at relatively large distances, these small lateral head movements would cause very minimal change of scenes, thus the fixed simulator scene is only minimally inaccurate.

The driving simulator produces a data stream which contains location and orientation information of all scriptable objects (including traffic such as oncoming cars) as well as location and orientation information of the driver's car based on a virtual
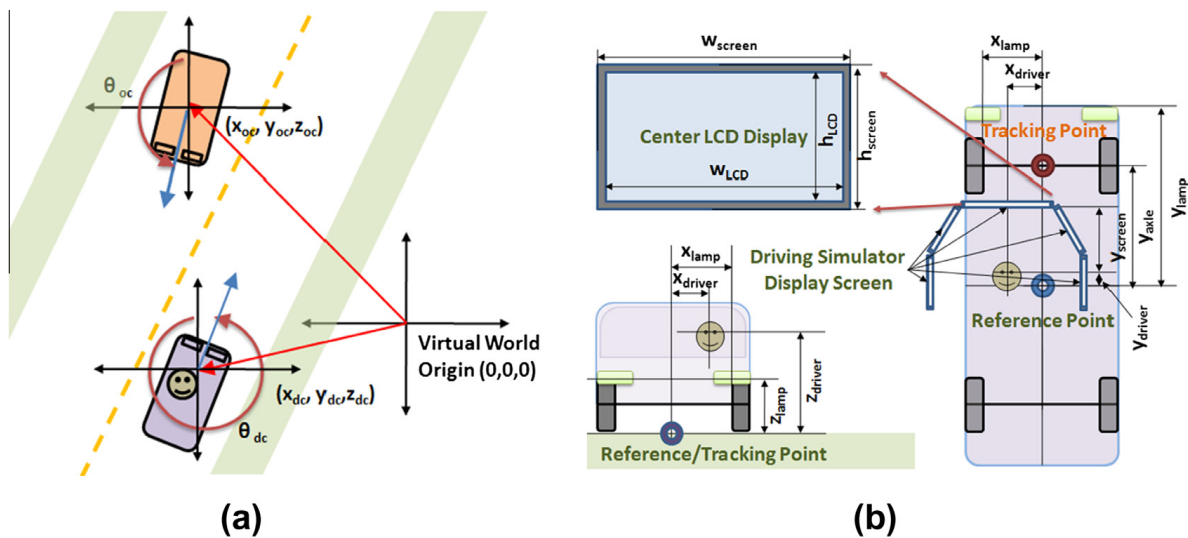

Fig. 2. Schematics of (a) driver's car and an oncoming car's locations and orientations measured in the virtual world coordinate system, as viewed from above. (b) Dimensions of the vehicle model and a scene projection configurations used in the various calculations.

world coordination system. The virtual world coordination system is a Cartesian coordinate system with respect to a pre-defined center of the virtual world (see Fig. 2a).

Note that a position of the scripted object (oncoming car) is based on the car model's reference point (a point between the centers of the front and rear axles), while the driver car's position is tracked by the center of the front axle (see Fig. 2b). Therefore, offsets for the headlamp positions and for the driver's viewing position from its reference/tracking point should be considered during the computation.

In order to find the headlamp positions projected on the screen in pixels, we first convert the virtual world coordinates of the oncoming car's headlamp positions to the relative spherical-polar coordinates centered at the pre-defined driver's head position. Then we compute the projected headlamp positions on a virtually-placed center screen. Finally, these positions in the virtual screen get converted to the integer pixel coordinates of the real world LCD screen using a mapping function between physical dimensions of the center screen ($W_{LCD} \times H_{LCD}$) and its native resolution (1366 pixels × 768 pixels).

Assuming that the oncoming car (OC)'s location is (x_{oc}, y_{oc}, z_{oc}) and its heading is θ_{oc}, and the driver's car (DC) is located at (x_{dc}, y_{dc}, z_{dc}) and its heading is θ_{dc} in the virtual world coordinate system, as shown in Fig. 2a, we can convert the headlight positions of an oncoming car using Eqs. (1)–(5).

First, we convert the oncoming car's headlight positions to a relative coordinate with respect to the driver's view point, (x_{LH}, y_{LH}, z_{LH}):

$$
\begin{aligned}
x_{LH} &= x_{oc} + x_{lamp} - (x_{dc} - x_{driver}) \\
y_{LH} &= y_{oc} + y_{lamp} - (y_{dc} - y_{axle} + y_{driver}) \\
z_{LH} &= z_{oc} + z_{lamp} - (z_{driver})
\end{aligned}
\tag{1}
$$

Then, we rotate the coordinate system based on driver's heading direction to get rotated coordinates, $(x'_{LH}, y'_{LH}, z'_{LH})$:

$$
\begin{aligned}
X'_{LH} &= x_{LH} \cdot \cos(\theta_{dc}) + x_{LH} \cdot \sin(\theta_{dc}) \\
y'_{LH} &= -y_{LH} \cdot \sin(\theta_{dc}) + y_{LH} \cdot \cos(\theta_{dc}) \\
z'_{LH} &= z_{LH}
\end{aligned}
\tag{2}
$$

Then we convert the Cartesian coordinates to the spherical-polar coordinates, (d, θ, ϕ), based on the driver's view point:

$$
\begin{aligned}
d &= \sqrt{x'^2_{LH} + y'^2_{LH} + z'^2_{LH}} \\
\theta &= \cos^{-1}\left(\frac{z'_{LH}}{\sqrt{x'^2_{LH} + y'^2_{LH} + z'^2_{LH}}}\right) \\
\phi &= \tan^{-1}\left(\frac{y'_{LH}}{z'_{LH}}\right)
\end{aligned}
\tag{3}
$$

where d is the Euclidean distance to the headlight position; θ is the horizontal rotation angle; ϕ is the vertical rotation angle.

This means that the Euclidean distance to the onscreen contact point is d'_{screen} as defined below. Now, we compute the projection of the headlamp location on the virtual driving simulator screen, (onscreen; $x'_{os}, y'_{os}, z'_{os}$). For ease of calculation, the spherical-polar coordinates of the contact point are converted back to Cartesian coordinates using the following equations:

$$
\begin{aligned}
d'_{screen} &= \frac{y_{screen}}{\cos(\theta) \cdot \sin(\phi)} \\
x'_{os} &= \frac{y_{screen}}{\tan(\phi)} \cdot \tan(\theta) \\
y'_{os} &= y_{screen} \cdot \tan(\theta) \\
z'_{os} &= \frac{y_{screen}}{\sin(\phi)}
\end{aligned}
\tag{4}
$$

Finally, by applying the conversion functions below, we can get the pixel coordinates of the headlamps center drawn on the central screen, (x_{os}, y_{os}):

$$
\begin{aligned}
x_{os} &= \frac{R_H}{2} + \frac{R_H \cdot x'_{os}}{w_{LCD}} \\
y_{os} &= \frac{R_V}{2} - \frac{R_V \cdot z'_{os}}{h_{LCD}}
\end{aligned}
\tag{5}
$$

where R_H is the horizontal native resolution of the screen (1366 pixels); R_V is the vertical native resolution of the screen (768 pixels).

Note that the data stream only contains heading (rotation around z-axis) information, and does not contain pitch (rotation around x-axis) or roll (rotation around y-axis) of scriptable objects (oncoming cars). This lack of information, in fact, can be problematic if the driver's car is on a flat road and an oncoming car is on an inclined/declined road because the real headlight positions will be affected by this unspecified oncoming car's self-rotation. On a typical two-lane road (4 m wide for each lane) with high incline/decline (50% grade = 26.57°), when the oncoming car is located at 50 m away from the driver, the projected vertical headlamp displacement due to the object pitch is less than 6 pixels. If the relative pitch value between the driver's car and the oncoming car is kept constant, the amount of displacement on the driving simulator's LCD screen increases as they approach to each other. However, this special case rarely happens on the real-world highways because

roads should be designed to avoid "broken back" (frequent change of incline/decline angle), and roads are recommended to have at least 400 feet (120 m) of tangent between two inclined/declined segments and transitions should be smooth and continuous (South Dakota Department of Transportation, 2011). Therefore, large pitch differences between two approaching cars only occur when they are far from each other. If they are separated enough, this displacement error will be small compared to the angular displacement caused by height differences between the cars. To further avoid that effect, the user should design scenarios that restrict the headlight glare encounters to only flat road segments.

3.2. Mapping onscreen pixel coordinates to LED-grid coordinates using view calibration

Our glare simulator only covers the central monitor, as glare from cars in the peripheral monitors is generally inconsequential. If we were able to follow the ideal component setup as shown in Fig. 1d, mapping onscreen pixels coordinates to the LED grid coordinate would be a simple linear conversion. Unfortunately, due to the physical constraints of the driving simulator, we cannot achieve this ideal alignment for every driver.

In order to superimpose an LED light from the LED grid over a headlight position on the LCD screen, the LED reflection should be projected on the LCD display plane as shown in Fig. 3a left. If the distance between the LED plane and the beamsplitter plane is bigger than the distance between the beamsplitter plane and the LCD plane (e.g., beamsplitter aligned at less than 45°), linear mapping of the LED reflection will fall behind the LCD plane, and this introduces parallax (see Fig. 3a right). Since there is a depth difference between the onscreen headlight position and the reflection of the LED, and the driver's position is relatively close to the central monitor, the alignment error (AE) is noticeable. The AE spreads over the simulated driving scene nonlinearly; the AE is minimized at the center of the scene and increases as the incident point to the LCD screen approaches the edge of the screen.

One way to reduce the AE caused by parallax is to develop and implement a fixed nonlinear mapping function between the LED and the LCD plane. However, a fixed solution is not practical, because seating position varies by driver and the angle of the beamsplitter may need to be changed to allow ergonomically comfortable driving space for individual drivers.

We resolve this alignment limitation using a simple calibration process performed by each driver before experiments start. It produces a set of spatial mapping coefficients between the driving simulator's onscreen surface and the LED grid surface. Since the full LED grid is composed of four 25×25 LED grid boards to form a 100×25 LED grid, with slight misalignments between the 4 boards, the drivers need to calibrate each LED board. During the calibration process, nine predefined LED positions on the LED grid are lit at a low brightness level (to minimize glare) and nine calibration dots appear on the driving simulator's central monitor, as shown in Fig. 3b. The driver is asked to drag each onscreen calibration dot to the center of the corresponding LED light position using a mouse. Once a driver finishes the task, the coordinates of the calibration dots (in pixels) as well as the corresponding LED coordinates are recorded. Spatial mapping is based on simple piecewise linear interpolation among calibration dots. The following equations convert onscreen pixel locations to corresponding LED grid coordinates (x_{LED}, y_{LED}):

$$x_{LED} = \left(\frac{x_{os} - x_{os\_L}}{x_{os\_R} - x_{os\_L}} \right) \cdot (x_{LED\_R} - x_{LED\_L})$$

$$y_{LED} = \left(\frac{y_{os} - y_{os\_D}}{y_{os\_U} - y_{os\_D}} \right) \cdot (y_{LED\_U} - y_{LED\_D})$$

(6)

where x_{os} is the horizontal pixel coordinate of a headlight position; x_{os_L} is the horizontal pixel coordinate of a nearest onscreen calibration point on the left; x_{os_R} is the horizontal pixel coordinate of a nearest onscreen calibration point on the right; x_{LED_L} is the horizontal LED coordinate of a corresponding LED on the left; x_{LED_R} is the horizontal LED coordinate of a
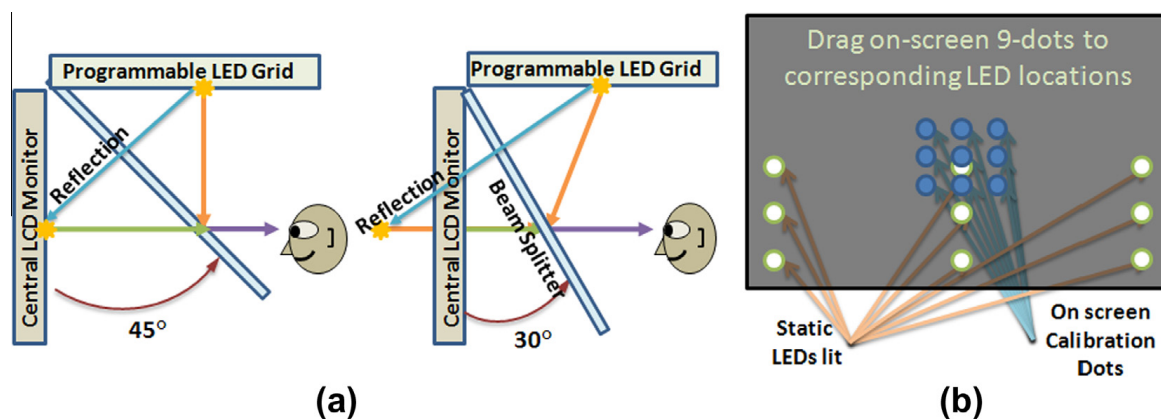
Fig. 3. Schematics of (a) LED reflection with ideal (left), and non-ideal (right) beamsplitter alignment. The different position/depth of the simulated position results in parallax. (b) Initial view of the drag-and-drop calibration process. The subject aligns the on screen dark blue spots to the corresponding positions of the 9 bright LED reflections using a mouse.

corresponding LED on the right; y_{os} is the vertical pixel coordinate of a headlight position; y_{os_U} is the vertical pixel coordinate of a nearest onscreen calibration point above (up); y_{os_D} is the vertical pixel coordinate of a nearest onscreen calibration point below (down); y_{LED_U} is the vertical LED coordinate of a corresponding LED above (up); y_{LED_D} is the vertical LED coordinate of a corresponding LED below (down).

In summary, since the driving simulator streams out the driver car position and the oncoming car position in virtual world coordinates during the run, we can use Eq. (1) through Eq. (5) to compute the onscreen headlight positions, and then apply Eq. (6) to compute the corresponding LED coordinate.

4. Simulation of real world headlight brightness

Along with keeping the spatial alignment between the LCD and LED screens, another, and possibly more vital part of a successful real world headlight simulation is assuring that the headlight glare system properly simulates the dynamics of real-world headlight brightness changes during a headlight glare encounter. The amount of headlight glare that would be perceived by a driver depends on the amount of light emitted from the oncoming headlight that reaches the driver's eye. Because a typical car uses headlamps designed to produce an anisotropic beam shape, the oncoming car's angular distribution of headlight intensity (beam shape) should be considered in addition to the distance and angle between a driver's car. Here we will briefly review the current beam shape regulations and related physical characteristics, and then describe how this headlight beam shape and cars' relative positions and orientations can be used to compute equivalent LED intensity levels needed to simulate the headlight level reaching the driver's eye.

4.1. Generic headlight beam shape

The U.S. National Highway Traffic Safety Administration (NHTSA) enforces the Society of Automotive Engineers (SAE) standard to reduce glare for oncoming traffic while ensuring sufficient light is emitted forward for safe driving at night (FMVSS, 2007). This regulation defines a set of cutoff values (low/high limits of projected brightness for headlights) in luminance intensity (candelas, cd), and it sweeps ±15° horizontally and ±5° vertically over a 2-dimensional angular projection surface. For regular low beam headlights, the brightest portion (peak) of the driver side headlamp should be aimed toward the lower-right to reduce the glare that oncoming traffic will sustain (see Fig. 4a). For high beams, headlights should be aimed straight ahead (0°V, 0°H). European countries follow the Economic Commission for Europe (ECE) standards which are conceptually similar to the SAE standards but designed to cause lower glare to oncoming traffic. The ECE standards for low beam allow more light toward the upper right to improve readability of road signs (ECE, 2006).

Although these cutoff values define maximum or minimum light intensities for some reference angle points, it is hard to generate a single mathematical model of a 'generic' headlight beam shape because headlight beam distribution is a complex angular function and it is different from manufacturer to manufacturer. Fortunately, a large survey of headlight beam shapes for the 20 top-selling passenger vehicles in the US and in Europe is available (Schoettle et al., 2001). In the survey, the luminous intensities at various angular locations were measured, covering ±45° horizontally and −5° to +7° vertically. The angular resolution of measurement points along the horizontal axis was unevenly spaced (0.5° between 0° and 5°, 1° between 5° and 10°, and 5° between 10° and 45°). Luminance intensity measures along the vertical axis were evenly distributed with an angular resolution of 0.5°.
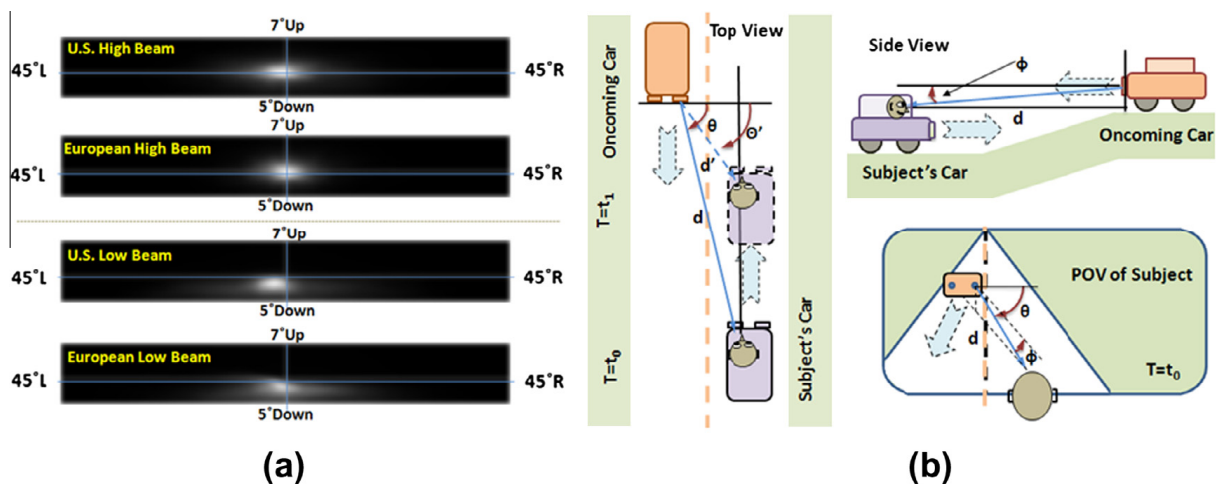

Fig. 4. (a) Angular distribution of projected light (averaged beam shape) for high and low headlight beams measured from the front, derived from (Schoettle et al., 2001). (b) Schematics of headlight projection angle calculation.

This variable resolution and discontinuity among measured points complicate the headlight glare simulator's LED brightness level calculations. In order to create a light distribution that is smooth and continuous, a bilinear interpolation was applied among neighboring data points to bridge the various spatial gaps between data points. Then a 2-dimensional fast Gaussian smoothing (with standard deviation of 0.5°) was applied to the light intensity distribution map to get a smooth headlight beam shape. The resulting smooth distribution map was sampled at a uniform angular resolution of 0.5°. Fig. 4a shows the resulting 'generic' headlight beam patterns in US and Europe, measured from the aiming direction.

Note that the brightness values (gray level) in Fig. 4a are normalized to a 0–255 range. Therefore, each plot shows the relative brightness distribution of a given headlight category instead of absolute/real measured values. The peak in the US high beam plot is located at (−0.5°H, 0°V), and the peak in the US low beam plot is located at (−3.5°H, −1.5°V).

The 75th percentile of measured luminous intensities at each angular position of the US low beam data was used to develop the headlight glare simulator specifications because it causes more glare than average luminance intensity, and thus keep the error on the side of having too much glare rather than too little. However, the software is designed in a modular way so that the system can accommodate the ECE standard or high beam conditions by simply replacing the beam shape map. Note that the 25th percentiles of measured luminance intensities are about half of the 50th percentile of measured luminance intensities, and the 75th percentile of measured luminance intensities are about twice the values of corresponding 50th percentile luminance intensities. Therefore, the overall variability of headlight brightness is at least factor of four.

4.2. Dynamics of luminance change

This Angular Light Intensity Distribution Map (ALIDM) offers a simple way to compute the required brightness intensity level (from an LED) needed for simulating headlight glare. The ALIDM assumes that the light source is infinitesimal and projects light from the center of a headlamp, regardless of actual headlamp size or shape. Since the pupil size is small (less than 5 mm with headlight glare) compared to the distance between the driver's eye and the headlight (usually more than 5 m), once we know the luminous intensity according to the ALIDM, the amount of light projected to driver's eye can be estimated by locating the projection point on the ALIDM and scaling it by projection distance.

For example, if a driver's car and an oncoming car are driving on parallel lanes towards each other, as shown in Fig. 4b, as the distance between the two cars (d) decreases, both the horizontal projection angle (θ) and vertical projection angle (ϕ) will vary. Note that the amount of light reaching the driver is inversely proportional to the distance squared (d^2). Since we can convert headlamp locations of oncoming cars to relative spherical-polar coordinates originating at the driver's point of view, we can compute the horizontal projection angles and the vertical projection angles.

Note that the vertical angle (pitch) difference between the oncoming car and driver car may greatly affect headlight brightness estimation. For example, if an oncoming car approaches the top of a shallow hill and the driver's car approaches the peak of the hill from the other side, the oncoming car's headlight, which is upward pointed, may cause more glare than when the encounter happens on a flat road. Unfortunately, the pitch information of the oncoming car is not available directly from the driving simulator's data stream. It is still possible to estimate the pitch of a car by computing the derivative of the car's height changes. Introducing headlight glare encounters on inclined/declined road makes the timing control during the scenario development and post data analysis much more complex. Therefore, we decided that the oncoming car's missing pitch information problem will be handled by scenario design, by limiting the glare encounters to flat road sections (or sections where both cars are on the same slope).

Once we know the projection angles, we can locate a corresponding relative brightness level from the ALIDM for modeled-world headlights. Finally, the amount of light projected to the oncoming driver's eye (L_{proj}) can be computed with the following equation:

$$\theta_{proj} = \frac{\pi}{2} - \theta$$
$$\phi_{proj} = -1 \cdot \phi \tag{7}$$
$$L_{proj} = \frac{ALIDM[\theta_{proj}, \phi_{proj}]}{d^2}$$

where d is the Euclidean distance to the headlight position; θ is the horizontal rotation angle; ϕ is the vertical rotation angle; θ_{proj} is the horizontal projection angle; ϕ_{proj} is the vertical projection angle.

4.3. Measuring LED beam shape and mapping of the brightness level

The last component in simulating real-world headlight brightness is the control of the correct amount of light with a high intensity LED. Similar to the consideration of headlight beam shapes in the previous section, we have to consider the beam shape of the LED itself, because the positioning (angular view) of LEDs affects the amount of light reaching the driver's eye. The LEDs used are the NSPW500DS white LED from Nichia (Tokushiba, Japan), and the manufacturer provided basic electrical/optical specifications for them. However, the information provided is not detailed enough to build a complete angular distribution model of the LED beam shape as we generated for the headlights. It is still possible to follow a measurement procedure similar to that used to build a headlight beam shape, as described in the headlight beam shape survey (Schoettle et al., 2001), to build an angular distribution of LED light intensity. However, we used a simpler but robust method to capture the LED beam shape using a digital camera.

One LED was lit at its maximum brightness and the LED board was placed on a flat surface, so that the LED was aiming directly upward. A glass plate was installed 0.1 m away from the LED, and a digital camera was set 0.5 m away from the LED. The camera was adjusted to aim straight down at the LED with all automated modes turned off (no auto exposure, no auto focus, no white balance, etc.). We placed a sheet of rectangular grid paper on the glass plate and manually adjusted the camera focus to get a sharp image of the grid. After taking a picture of the spatial grid, the grid paper was replaced by a neutral density (ND) filter, and we took a picture of the projected beam shape on the ND filter with ambient room light turned off. The optical density of the filters applied was increased gradually in log steps of 0.3 until pixel saturation (whiteout portion of the picture) disappeared. Note that each addition of 0.3 in density results in reduction of 50% of light transmittance. Since all of the pictures were taken at the same location, the same spatial coordinates apply to each picture that captures the spatial distributions of the light.

A pixel substitution algorithm was applied for integration of the images taken. First, the algorithm searched for saturated pixels from the non-ND filtered image, and then replaced those pixels with 'spatially' corresponding pixels from the next level ND filtered image. When a saturated pixel is substituted, the white level of the pixel needs to be adjusted to compensate for the light reduction attributed to the ND filter. The following conversion function recovers the pixel value.

$$v_{recovered} = 255 + v + \frac{v}{(100 - r)} \cdot r \tag{8}$$

where $v_{recovered}$ is the corresponding pixel value recovered from the ND filtering; v is the corresponding pixel value of the next level ND filtered image; r is the percent reduction of light caused by an ND filter.

For example, if a saturated pixel (pixel value of 255 in an 8-bit grayscale image) in a non-filtered image is replaced by a corresponding pixel with a pixel value of 10 in the next level ND-filtered image, the resulting recovered pixel value is 20. This value should be added to the previous maximum pixel value (255), so the final pixel value becomes 275.

After processing of each ND-filtered image iteratively, the pixel values were normalized to the range of 0–255 before continuing the pixel substitution process for the next level. Finally, a Gaussian smoothing of SD = 0.5° was applied to produce a final angular light distribution map for the LED, and the angular coordinates of pixel locations were computed from the picture of the rectangular grid.

This dynamic range photography is conceptually similar to the high dynamic range imaging (HDRI) technique, used to overcome overexposure problems of single exposure setting (McCann and Rizzi, 2011). It enabled us to measure the full brightness range of the LED, which is much higher than a regular camera can capture, and its spatial distribution (beam pattern). The result of this measurement is shown in Fig. 5a.

The centered high brightness beam shape of the LED indicates that LEDs located farther from the center of the screen need to produce more light than the ones located near the center of the screen to provide the same amount of required brightness level to the driver.

Since we already have a mapping function between the on-screen positions and the LED grid coordinates, as well as pixel pitch of the LCD screen (1375.4 pixel/m), and single LED grid width (0.006 m) of the LED boards, we can compute the beamsplitter angle (ω) by computing the arctangent of the ratio between the physical distance of two onscreen calibration positions along the vertical center line and distance between corresponding LED locations (see Fig. 5b left).

$$\omega = \arctan \left(\frac{d_{os}}{d_{LED}} \right) = \arctan \left(\frac{h_{LCD} \cdot (y_{LCD\_U} - y_{LCD\_D})}{h_{LED} \cdot (y_{LED\_U} - y_{LED\_D})} \right) \tag{9}$$
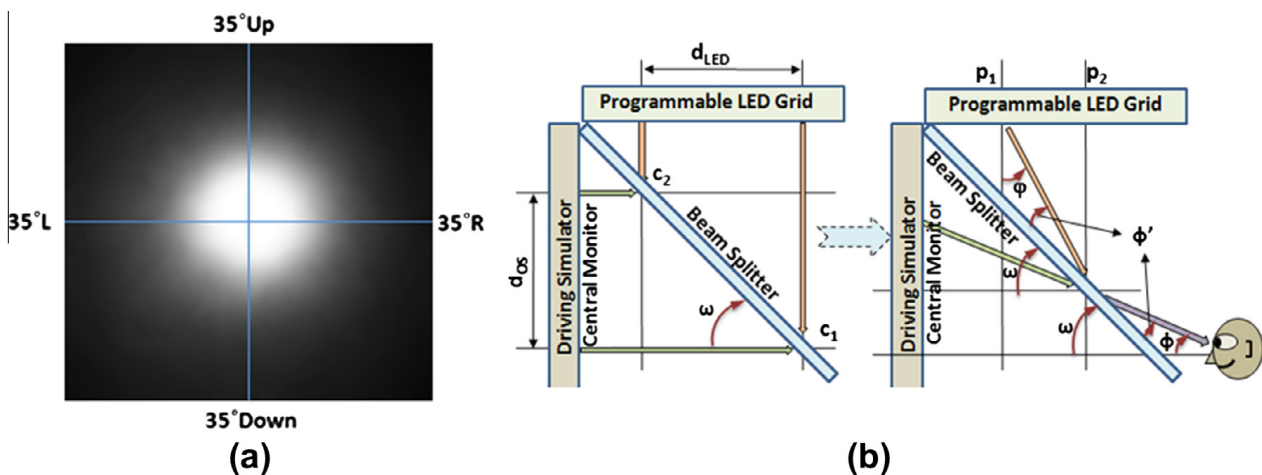
Fig. 5. (a) Angular light distribution of an LED generated by dynamic range photography using series of neutral density filters. Note that the LED beam shape is circular. (b) Schematic of the light projection angle calculation for an LED. The beamsplitter angle (ω) is the arctangent of the distance ratio between two vertical onscreen calibration positions, and between corresponding LED locations (b-left). The LED projection angle (φ) (b-right) is computed using Eq. (10).

where h_{LCD} is the height of a pixel on the LCD screen (0.000681 m); h_{LED} is the height of an LED on the LED grid (0.006 m); y_{LCD_U} is the vertical coordinate of the upper calibration dot position; y_{LCD_D} is the vertical coordinate of the lower calibration dot position; y_{LED_U} is the vertical coordinate of the corresponding upper calibration LED position; y_{LED_D} is the vertical coordinate of the corresponding lower calibration LED position.

Once we know the beamsplitter angle, we can compute the LED projection angle (φ) using Eq. (10) and estimate the LED brightness level in a manner similar to the one used for the headlight beam shape computation (see Fig. 5b right).

$$\phi' = 180 - (180 - \omega) - \phi$$
$$\varphi = 180 - (\omega + \phi') = 180 - 2 \cdot \omega + \phi$$

(10)

where ϕ is the vertical component of the driver's viewing angle of the LED.

Note that the additional computations shown here are needed for estimating the vertical component of LED projection angle because the beamsplitter was hinged horizontally, permitting vertical swings. The horizontal component of the LED projection angle can be computed directly from the horizontal angle to the onscreen headlight position.

It is also necessary to take into account that the beamsplitter used has an optical characteristic of 58R/42T which means that only 58% of the light produced by the LED is delivered to the driver's eye. Therefore, the final brightness level of the LED should be 1.72 times higher than the required LED brightness modulated by the angular brightness distribution map of the LED discussed above.

However, the manufacture's specified R/T ratio is measured with a light incident angle of 45°, and it is expected that the R/T ratio will vary with different light incidence angles. To check the variability of the R/T ratio, measurements were conducted. The light source (table lamp) is placed 50 cm away from the beamsplitter, and angled at 15°, 30°, and 45° from the normal of the beamsplitter. Peak luminances of reflected light were measured from 50 cm away from the beamsplitter using a Minolta LS-100 luminance meter. The peak luminance of reflected light is about 5000 cd/m^2 with 15° incidence angle, 4900 cd/m^2 with 30° incidence angle, and 4800 cd/m^2 with 45° incidence angle. This means that there is about 2% of reflection reduction per 15° incidence angle changes. Since the incidence angle from the LED board to beamsplitter varies 45–18.5° vertically and 0–30° horizontally, the simulated headlight brightness is over-produced most of time. However, the brightness simulation error caused by incidence ratio change will be less than 4%, a brightness difference that is non-detectable with the human eye.

4.4. Programmable LED board and spatial and brightness quantization

The early prototype of the glare simulator (Fullerton and Peli, 2009) used an off-the-shelf programmable LED display board with sparsely populated LEDs (low spatial resolution). Consequently, when the smooth headlight movements on the driving simulator screen (high spatial resolution) are simulated by the selection of the LED light on the board, the simulated headlamps appeared to move discontinuously due to the large spatial gaps between LEDs on the board (quantization error – aliasing). In order to reduce these jumping movements, we ordered customized LED boards which are about 1/4 the size of the original board while holding the same number of LEDs in a 25×25 square grid at the maximum LED spatial density. These new LED boards allow smoother headlight motion simulation. However, due to the reduced size and dense packing of the LED grid, 4 LED boards are required simultaneously to cover the full simulator display area.

Each LED board contains an ATmega328P microcontroller, two STP16DP05 LED driver chips and a USB/Serial interface to a PC. The boards are controlled by the Arduino-compatible Peggy2Serial library. For real-time communication to the board, the Java RXTX serial/parallel communication library is used. The brightness level of individual LEDs depends on the number of positive current pulses supplied to the LED in a given period of time. For example, if there are 375 cycles of current pulses available in a second, but no current is supplied to the LED during the entire time, the perceived brightness will be the darkest (turned off). If the current is always supplied during the entire time, the perceived brightness will be brightest (turned on). If every other current pulse is supplied to the LED, the LED brightness will be half of its maximum brightness. It is possible to produce up to 376 brightness levels with the method described above, but due to the hardware limitations of the interrupt frequency, and the frame rate (at least 24 fps) required for LED animations, the number of brightness levels available for the current implementation of the programmable LED board is limited to 16 levels. This means that the required brightness level derived from the previous calculations needs to be quantized into 16 levels.

Although it depends on luminance difference between successive steps and on duration of each step, simulation of perceptually continuous brightness change using discontinuous stepping (quantized) brightness levels is certainly possible (Vicario and Zambianchi, 1999). In our implementation, since the brightness change during the simulation is in fast pace, and the luminance difference between each successive step is relatively small (6.25% change between frames) at the high operational brightness levels (about 20,000 cd/m^2), the perceptual transition of brightness change appears smooth.

4.5. Simulation of real-world headlight size

Another dynamic factor which might be important for simulating the real-world headlight is the dynamic changes of the glare source angular size. The driver's perception of the visible size of the glare source (headlamp) increases as the oncoming

car approaches the driver's car. For example, if an oncoming car approaches and reaches about 7 m away from the driver's car, a regular-sized headlight (0.1 m × 0.3 m) covers about 0.82° × 1.22° of driver's visual angle.

However, simulation of the gradual size change requires a much finer spatial resolution LED grid than the current LED board provides. For the case of larger expansion of headlight size (when an oncoming car is close to the driver's car), we considered using multiple adjacent LEDs to be lit while keeping the total amount of light from individual LEDs to the driver's eye to be as required. However, because of the relatively coarse spatial resolution of the LED board (each LED covers 0.45° in visual angle), multiple LEDs lit look like multiple glare sources instead of the single glare source as one perceives from car headlight. Fortunately, a previous headlight glare study using static real world glare sources reported that the size of glare source does not affect the peripheral detection performance of the driver (Bullough et al., 2003). Therefore, we decided to use a single LED to simulate a single headlight regardless of its size variation. LED based car headlights may include multiple LEDs and those may be visible to oncoming cars. When that practice becomes more common our simulator can be adjusted to represent such headlights.

5. Simulator performance

5.1. Spatio-temporal synchronization

Although the glare simulator employs tightly packed LED grids, spatial resolution of the LED grid is much coarser than that of the LCD screen, and that inevitably introduces spatio-temporal synchronization errors. Motion of the LED lights appears discrete and discontinuous, and more so when the oncoming car is far away where the movements of oncoming cars visible to the driver are relatively slow, but may cause a transition from an LED position to neighboring LED position (aliasing). Fig. 6a illustrates an example of a case where a small transition of mapped headlight points transverse the borders of neighboring LEDs causing large discrete movement. In this case, the spatio-temporal synchronization error will be half of a LED size (0.225° in visual angle) over a video frame time.

Another artifact of the low spatial resolution of the LED grid is that when we use a simple nearest neighbor selection algorithm to choose a corresponding LED to be lit, the movements of an LED light appear stepped if the mapped headlight position takes a diagonal path on the LED grid, as shown in Fig. 6b. This stepping effect is more noticeable when the oncoming car is far and makes relatively slow movements. To minimize this motion artifact, a spatio-temporal buffer algorithm has been implemented so that when a mapped headlight position falls into the middle area among four neighboring LEDs, the decision of a new LED position is postponed, and the current LED position is kept until a more definitive LED position is computed (Fig. 6c). Note that although the spatial position of the LED doesn't change during this buffering process, the LED changes its brightness corresponding to the real-world condition. Although the implementation of this algorithm results in a visually smoother motion path of LED transition, the spatio-temporal synchronization error may build up to 0.35° in visual angle over a few frames.

All of these spatio-temporal synchronization errors are much less noticeable as oncoming traffic approaches the driver, where the visible movements of the oncoming traffic's headlights are large. In this fast-moving condition, temporal-spatial buffering may result in a large error if the consecutively mapped headlight positions on the LED grid fall within the buffering area. Therefore, the spatio-temporal buffering has a threshold of 0.35°, such that if the consecutive mapping of two points is
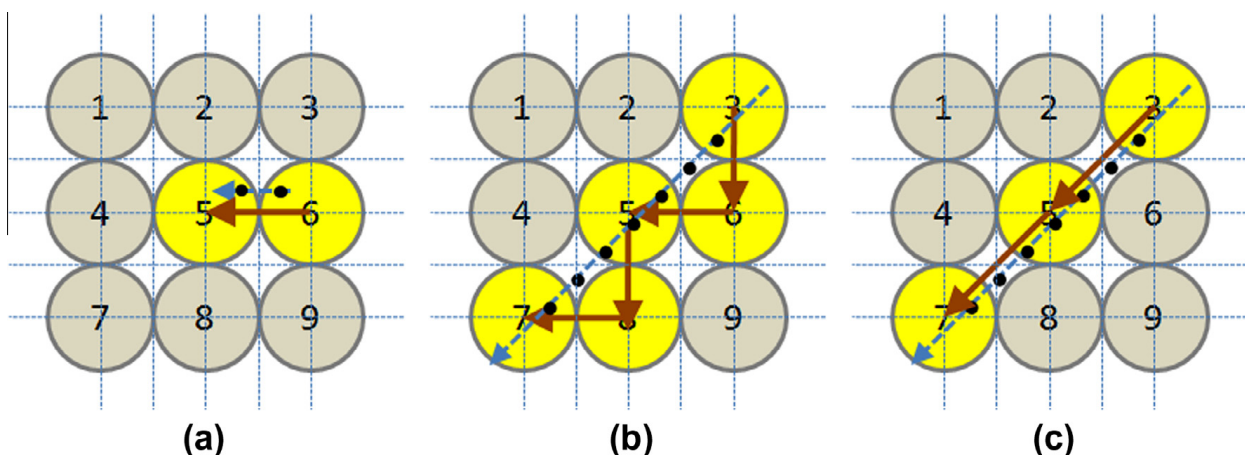
Fig. 6. Illustration of the aliasing limitations of the LED grid. (a) The case where a small transition of mapped headlight points between the edges of two LEDs creates a large spatial mapping error compared with the virtual world change in position. Black dots represent the series of computed headlight positions. (b) Diagonal headlight movements (small black dots) may cause a stepping LED motion when mapped. (c) With spatio-temporal buffering, LED motion for the same headlight motion is smoother and remains on course.

more than the threshold, the system switches back to the simple nearest neighbor finding algorithm to choose the corresponding LED. That adjustment eliminates the error during fast movement of headlights.

5.2. Headlight brightness changes synchronization

Spatio-temporal synchronization involves multiplexing of two light sources (LED and LCD) so that the viewer from the driving seat perceives those as a single light source in time (e. g. without parallax between LED and LCD position). However, from the research perspective the more important factor may be how closely the amount of light simulated by the glare simulator is similar to the real-world condition, while a slight spatial mislocalization may have little effect.

Fig. 7a shows plots of typical horizontal and vertical projection angle changes from the headlight (with 2 m, 3 m, and 4 m inter-vehicle lateral gap) using computer modeling of conditions. As two cars are approaching each other, the projection angle slowly increases with approach distance until the distance is around 25 m (less than 10°H and less than 3°V change) then rapidly increases. Corresponding luminance changes that a driver perceives when two cars are approaching each other on a two-lane road with various inter-vehicle lateral gaps, which are based on the generic headlight model, are shown in Fig. 7b. It follows a similar pattern as the projection angle changes. However, the required brightness rapidly drops around the 10 m approach distance because the headlight beam shape is focused at a lower right direction. The highest luminance level for each illustrated lateral separation is 11,235 cd/m^2 for 2 m inter-vehicle lateral gap, 7114 cd/m^2 for 3 m gap, 4042 cd/m^2 for 4 m gap, and it happens when the projection angle is 12.5°(H)–5.0°(V), 20.5°(H)–5.6°(V), and 24.0°(H)–5.0°(V), respectively.

Fig. 7c shows luminance changes for two common bypassing conditions (2 m and 3 m gap) measured with a real-world oncoming car (2012 VW beetle). The car was parked with its low beam headlights on, and the luminances were measured along the passing path using a Minolta LS-100 luminance meter at a regular driver-eye level (1.2 m), every 5 m of approach distance. It can be observed that a real world (recent) headlight design has better design of the headlight beam shape, as it produces more light towards the forward direction at far distances, but oncoming drivers will experience lower peak luminance at the close distance than the peak luminance expected from our generic headlight model. Although there are differences in luminance change between the generic headlight model (based on the 2001 surveys) and recent real-world measurements, the error is less than a factor of 2 and thus it is not larger than differences in various headlamp designs. Note
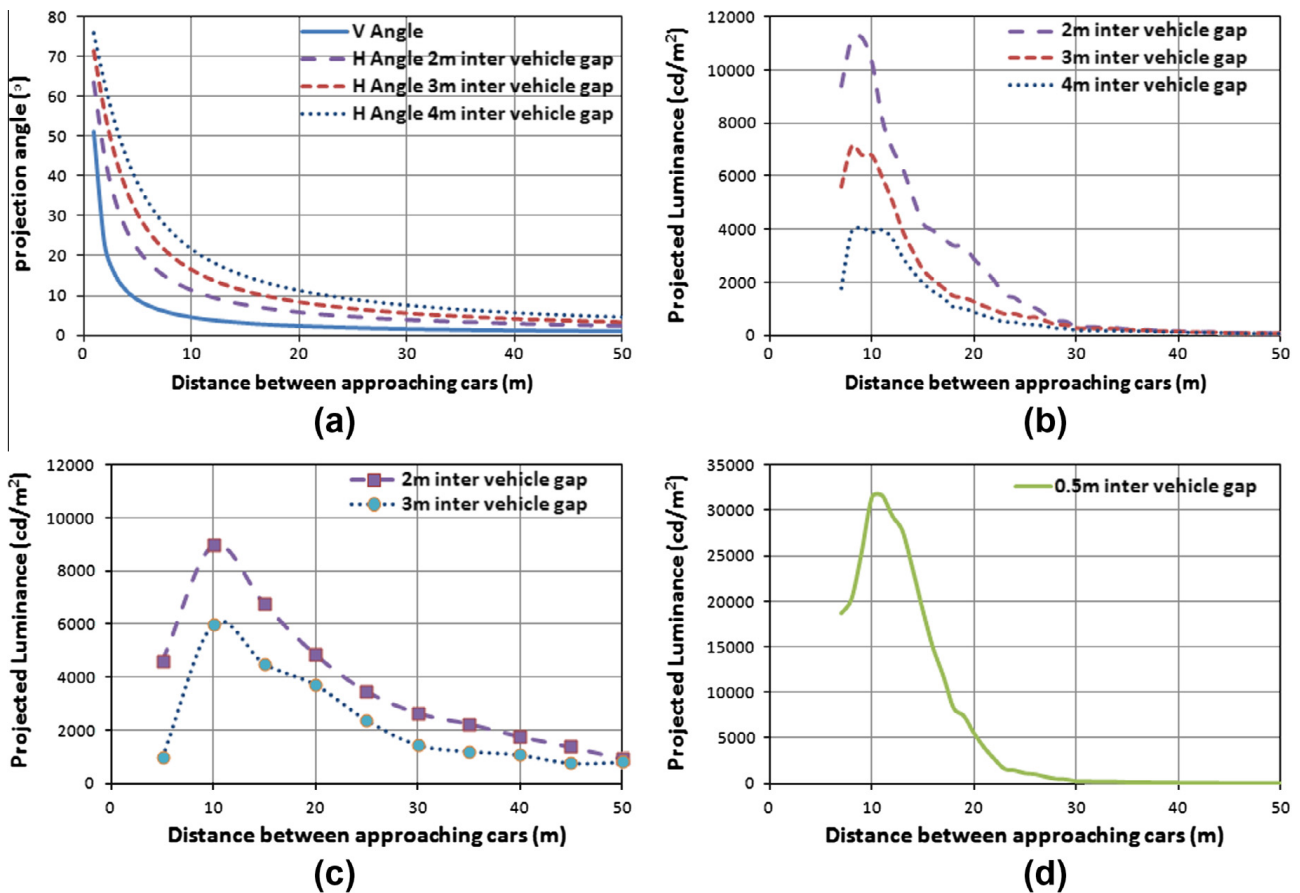

Fig. 7. Plots of (a) calculated horizontal and vertical projection angle changes from the oncoming car with 2 m, 3 m and 4 m inter-vehicle lateral gaps, and (b) corresponding expected luminance changes projected to the driver eye, when two cars are approaching each other from 50 m on a flat 2-lane road, based on generic headlight beam pattern. (c) Comparable luminance changes measured with a real-world car headlight with 3 m and 2 m inter-vehicle lateral gaps. (d) Luminance change of an extreme case, close call of bypassing (0.5 m inter vehicle gap).

that when the luminance is measured with Minolta LS-100, if the oncoming car is located farther than 20 m, the size of the headlight becomes less than 1°, and this results in systematic underestimation of measured brightness because the luminance meter integrates the total received light in the central 1° of receptive field to compute luminance. However, it seems that this measurement error is also smaller than variations among different headlight lamps.

The assumptions used to generate the plots in Fig. 7a–c do not represent the absolute worst glare case that can possibly happen because the horizontal projection angle does not cross the maximum peak projection angle (−3.5°H, −1.5°V). Although this special case can happen if two cars are approaching each other on a curved hill, it is hard to get to this extreme because of the incline-decline limitation of road design, and safe distance between two cars. A more realistic extreme case will be a near miss ("close call") of a head-on collision, which can be simulated as the passing gap between two cars being very close (0.5 m). In this case, the peak of the required luminance goes up to 31,679 cd/m², at 2.6° (H), 4.1° (V), and 11 m away from the driver (see Fig. 7d).

Note that beam shape is defined within ±45° (H) and −5° to 7° (V) range, so, the luminance requirement cannot be computed once the headlight projection angle goes beyond these ranges. In this case, the luminance level of the LED will remain fixed until the oncoming car passes by.

5.3. Simulation of real-world headlight

Luminance mappings are based on the relative peak brightness of the 'generic' headlight and the LED. This means that the LED used should be able to produce enough light to simulate the same amount of light produced by the oncoming traffic's headlight that is reaching the driver's eye. In order to verify the simulation, the peak luminance of 5 LEDs and 3 real-world headlights were measured using the Minolta LS-100 luminance meter. The average peak luminance of the LEDs at 1 meter away was 47,221 cd/m², and the average peak luminance of the real-world headlights at 2 m away was 104,051 cd/m². This means that if the headlight luminance were measured at the same distance (1 m), the real-world headlights produce about 8.8 times brighter light (416,204 cd/m²) than the LEDs used. However, since the LEDs are installed about 0.74 m away from
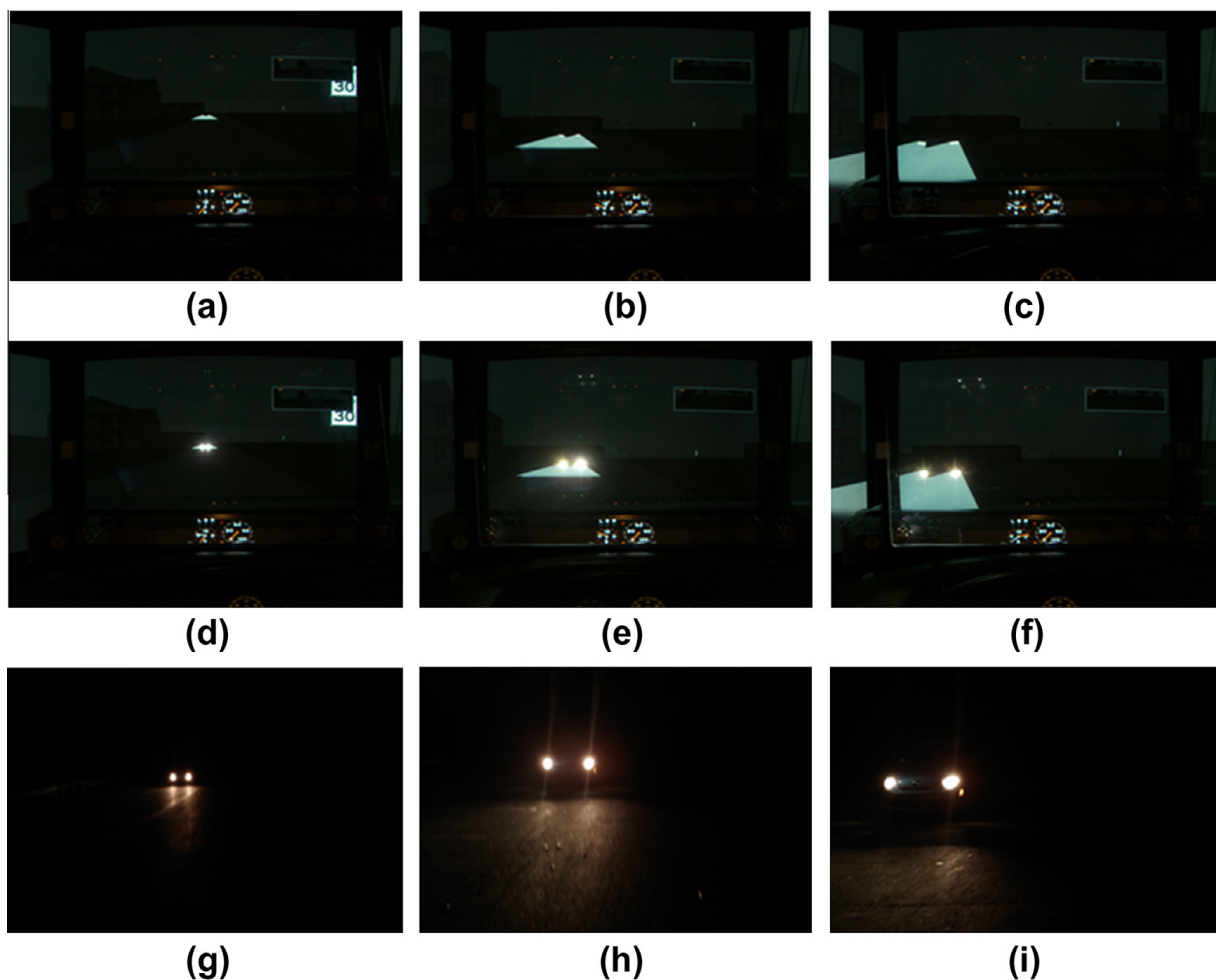
Fig. 8. Photographs of the simulation of night driving on a driving simulator. (a–c) Without the headlight glare simulator. (d–f) With the headlight glare simulator turned on. (g–i) Corresponding real-world photographs of staged nighttime headlight glare scene. The three simulations represent three approach distances between the cars.

the driver in the driving simulator, and the real-world headlight reaches its peak level no nearer than 7 m while driving, the operational capability of the LEDs for delivering the required level of light to the driver is about 5.6 times higher than what is required. Even if we consider the luminance reduction due to the beamsplitter, the LEDs are able to deliver 3.25 times brighter light to the subject. Note that this peak luminance comparison is based on the most extreme case that the oncoming car's headlight is 1 m away from the driver's eye, and aiming at the driver, which is impossible in real-world driving condition. Therefore, we conclude that our LEDs are sufficient for simulating real-world headlight brightness.

A simulation error for brightness synchronization can be caused by two factors, one from LED light quantization, and the other from the discrepancy between real-world headlight beam shapes and the generic headlight beam shape. However, as mentioned before, the combined simulation error remains under a factor of two, a level hardly detectable by human observer. Therefore, our simulation of headlight glare seems visually plausible and realistic.

Fig. 8a–c shows the driving simulator view without the headlight glare simulator activated using a photograph of the screen-beamsplitter combination. Fig. 8d–f shows a photograph of the screen-beamsplitter combination with the headlight glare simulator activated. Corresponding real-world photos of a nighttime scene are shown in Fig. 8g–k. Note that a camera is also affected by headlight glare in similar way to a healthy normal eye (McCann and Rizzi, 2011).

6. Summary

We described a novel headlight glare simulator using programmable LED display boards and a beamsplitter plate that can be installed on an existing driving simulator. The LEDs on the board produce brighter lights than conventional LCD displays can produce. The successful simulation depends on how well a glare simulator can synchronize the spatial movements of the oncoming headlight positions with LED illumination sequence and how well a glare simulator mimics the corresponding real-world headlight brightness perceived by a driver, which varies based on spatial positioning of a driver's car and oncoming traffic.

For spatial alignment, we have employed a simple intuitive calibration method to get a spatial mapping function between virtual world coordinates and the LED grid coordinates. During a drive in the driving simulator, the system computes the coordinates of LEDs to be lit using the calibration mapping function based on a real time data stream from the driving simulator. For accurate LED brightness simulation, the real-world beam shapes of a 'generic' headlight as well as the beam shape of the LED were considered when computing the corresponding LED light level. The range of headlight brightness required for the simulation of the worst glare case has been analyzed to ensure the validity of the headlight simulation. Note that although we were able to show that the simulation error of each simulation component is negligible and at most barely noticeable, due to the dynamic complexity (spatial and temporal) of the headlight glare level changes during the simulation, the estimated performance error shown in this paper may be limited as a validation of whole system. Also, manufacturing errors of the simulator parts, such as LEDs and beamsplitter, may affect the simulation performance. However, considering the wide variety of beam shapes and strengths of headlamps existing in real world, we conclude that the operational performance errors will remain well below the variations among real-world headlamp.

The system needs to be validated further through various behavioral comparison and subjective questionnaire studies. For an ideal testing condition, subjects perform a pedestrian detection task while driving a real car and being exposed to the real-world headlights in a controlled course. Then the same drivers perform the same task under comparable conditions in a driving simulator with the headlight glare simulator. Subjects also rate the perceived glare similarity of the real drives and the headlight glare simulator. By comparing the detection and driving performance between those two experimental conditions, and analyzing the subjective ratings of glare simulator performance, we can further increase our confidence in the validity of the headlight glare system.

With the safe and repeatable nature of driving simulator studies, and the development of a realistic headlight glare simulator such as the one shown here, we open new opportunities to study the effects of headlight glare during nighttime driving conditions. For example, this can be used to evaluate the nighttime driving of older people with and without vision impairments and their treatments (especially cataracts) and to address the safety of ophthalmic devices (e.g., multifocal intraocular lenses) to determine if they impair or aid nighttime driving. The results of those studies will provide evidence to impact future decision-making in determining nighttime driving privileges and restrictions imposed on people with vision impairment (Peli and Peli, 2002).

References

Akashi, Y., Rea, M., 2001. The effects of oncoming headlight glare on peripheral detection under a mesopic light level. In: Proceedings of the Progress in Automobile Lighting Symposium. Darmstadt University of Technology, Darmstadt Germany, pp. 9–22.
Akutsu, H., Legge, G.E., Luebker, A., Lindstrom, R.L., Zabel, R.W., Kirby, V.M., 1993. Multifocal intraocular lenses and glare. Optom. Vis. Sci. 1993 (70), 487–495.
Bhise, V., Meldrum, J., Jack, D., Troell, G., Hoffmeister, D., Forbes, L., 1981. Driver head movements in left outside mirror viewing. SAE Tech. Pap. 810761, 1981. http://dx.doi.org/10.4271/810761.

Bullough, J.D., Fu, Z., Van Derlofske, J., 2002. Discomfort and Disability Glare from Halogen and HID Headlamp Systems. Advanced Lighting Technology for Vehicles, SAE SP-1668. Paper # 2002-01-0010.

Bullough, J.D., Van Derlofske, J., Dee, P., Chen, J., Akashi, Y., 2003. An Investigation of Headlamp Glare: Intensity, Spectrum and Size. DOT#80, Washington: U.S. Department of Transportation, National Highway and Traffic Safety Administration.

Bullough, J.D., Skinner, N.P., Pysar, R.M., Radetsky, L.C., Smith, A.M., Rea, M.S., 2008. Nighttime Glare and Driving Performance. Research Findings. DOT# HS-811-043. U.S. Department of Transportation, National Highway and Traffic Safety Administration, Washington.

Collins, M., 1989. The onset of prolonged glare recovery with age. Ophthalmic Physiol. Opt. 9, 368–371.

De Waard, P.W., Jspeert, J.K., Van de Berg, T.J., De Jong, P.T., 1992. Intraocular light scattering in age-related cataracts. Invest. Ophthalmol. Visual Sci. 33 (3), 618–625.

Economic Commission for Europe (ECE), 2006. ECE 112: uniform provisions concerning the approval of motor vehicle headlamps emitting an asymmetrical passing mean or driving beam or both and equipped with filament lamps. Regulation § 112.

Federal Motor Vehicle Safety Standard (FMVSS), 2007. Federal Motor Vehicle Safety Standard #108: Lamps, Reflective Devices, and Associated Equipment. Code of Federal Regulations, Office of the Federal Register, DC, Washington, § 571.108.

Flannagan, M.J., 1999. Subjective and Objective Aspects of Headlamp Glare: Effects of Size and Spectral Power Distribution. University of Michigan Transportation Research Institute, UMTRI-99-36. The University of Michigan Transportation Research Institute, Ann Arbor, MI.

Fullerton M., Peli E., 2009. Development of a system to study the impact of headlight glare in a driving simulator. In: Proceedings of the 5th International Driving Symposium on Human Factors in Driver Assessment, Training and Vehicle Design, Montana, USA, pp. 412–418 (June 22–25).

McCann, J.J., Rizzi, A., 2011. HDR in Natural Scenes, in The Art and Science of HDR Imaging. John Wiley & Sons, Ltd., Chichester, UK. http://dx.doi.org/10.1002/9781119951483.ch3.

Miller, D., Benedek, G., 1973. Intraocular Light Scattering: Theory and Clinical Application. Charles C. Thomas, Springfield, Illinois.

Owens, D.A., Brooks, J.C., 1995. Drivers' Vision, Age, and Gender as Factors in Twilight Road Fatalities. University of Michigan Transportation Research Institute, UMTRI-95-44. The University of Michigan Transportation Research Institute, Ann Arbor, MI.

Owsley, C., McGwin Jr., G., Searcey, K.A., 2012. Population-based examination of the visual and ophthalmological characteristics of licensed drivers aged 70 and older. J. Gerontol. A Biol. Sci. Med. Sci.. http://dx.doi.org/10.1093/gerona/gls185.

Peli, E., Peli, D., 2002. Driving with Confidence. A Practical Guide to Driving With Low Vision. P.192. World Scientific, Singapore.

Plainis, S., Murray, I.J., Charman, W.N., 2005. The role of retinal adaptation in night driving. Optom. Vis. Sci. 82, 682–688.

Sandberg, M.A., Gaudio, A.R., 1995. Slow photostress recovery and disease severity in age-related macular degeneration. Retina 15 (5), 407–412.

Schoettle, B., Sivak, M., Flannagan, M.J., 2001. High-beam and Low-Beam Headlight Patterns in the US and Europe at the Turn of the Millennium. University of Michigan Transportation Research Institute UMTRI-2001-19. University of Michigan Transportation Research Institute, Ann Arbor, MI.

Shi, W., Lockhart, T.E., Arbab, M., 2008. Tinted windshield and its effects on aging drivers' visual acuity and glare response. Saf. Sci. 46, 1223–1233.

Sjostrand, J., Abrahamsson, M., Hard, A.L., 1987. Glare disability as a cause of deterioration of vision in cataract patients. Acta Ophthalmol. Suppl. 182, 103–106.

South Dakota Department of Transportation, 2011. Road Design Manual: Chapter 6-Vertical Alignment. SDDOT Chapter 6, USA, June 22–25, pp. 412–418.

Stringham, M.J., Hammond, B.R., 2008. Macular pigment and visual performance under glare conditions. Optom. Vis. Sci. 85, 82–88.

Sullivan, J.M., Flannagan, M.J., 2002. The role of ambient light level in fatal crashes: inferences from daylight saving time transitions. Accid. Anal. Prev. 34, 487–498.

Vicario, G.B., Zambianchi, E., 1999. On Continuity Perception in Brightness Change. Perception, 28 ECVP Abstract Supplements.

Van den Berg, T.J., Van Rijn, L.J., Kaper-Bongers, R., Vonhoff, D.J., Volker-Dieben, H.J., Grabner, G., Nischler, C., Emesz, M., Wilhelm, H., Gamer, D., Schuster, A., Franssen, L., de Wit, G.C., Coppens, J.E., 2009. Disability glare in the aging eye: assessment and impact on driving. J. Optom. 2, 112–118.

Winther-Nielson, A., Corydon, L., Olsen, T., 1993. Contrast sensitivity and glare in patients with a diffractive multifocal intracular lens. J. Cataract Refract. Surg. 19, 254–257.

Wood, J.M., Tyrrell, R., Chaparro, A., Marszalek, R., Charberry, T., Chu, B.S., 2012. Even moderate visual impairments degrade drivers' ability to see pedestrians at night. Invest. Ophthalmol. Vis. Sci. IOVS-11-9083.